Mixing Does the Magic: A Rapid Synthesis of High Surface Area Noble Metal Nanosponges Showing Broadband Nonlinear Optical Response

Katla Sai Krishna,[†] C. S. Suchand Sandeep,[‡] Reji Philip,[‡] and Muthusamy Eswaramoorthy[†,*]

[†]Nanomaterials and Catalysis Lab, Chemistry and Physics of Materials Unit, DST Unit on Nanoscience, Jawaharlal Nehru Centre for Advanced Scientific Research, Bangalore, India 560064 and [‡]Light and Matter Physics (LAMP) Group, Raman Research Institute, Bangalore, India 560080

ABSTRACT Here we report an instantaneous formation of high surface area metal nanosponges through a one-step inexpensive method in a completely green solvent, water. Merely by optimizing the concentration of the precursors and the reducing agent, we were able to generate a three-dimensional porous structure made up of nanowire networks. This is a general process, involves a simple, room temperature reduction of metal salts with sodium borohydride, and is therefore scalable to any amount. Further, these nanoporous metals because of their network structures show optical limiting behavior of a true broadband nature that would find applications in optoelectronic nanodevices.

KEYWORDS: nanosponges · porous nanostructures · noble metals · optical limiting · SERS

Porous metals with sponge-like nanostructures, for their high surface area, low density, high gas permeability, and thermal conductivity, find immense applications in catalysis,[1] fuel cells,[2,3] membranes,[4] sensors,[5,6] electrodes,[7] and actuators.[8,9] Though significant progress has been made in making and manipulating many porous, high surface area metal oxides,[10−12] the same is not true for the metals. The most versatile template-based approach used for the synthesis of porous, high surface area metal oxides does not give the desired results with metals, in particular, noble metals such as Ag, Au, Cu, Pt, and Pd, which are industrially more valuable considering their use in the production of hydrogen from methane,[13] reduction of pollutants from automobiles,[14] CO oxidation,[15−17] and in fuel cells.[2,3] Nevertheless, template-based methods employing both soft and hard templates were routinely used to make porous noble metals with very low surface area (<2 m^2/g).[18−22] Other methods such as selective dissolution of a metal from an alloy,[23,24] pH-controlled reduction by glucose,[25] fusion of nanoparticles at the interface of a biphasic oil−water mixture,[26] reaction-limited aggregation,[27] and emulsion-based synthesis in presence of a surfactant[28] were also used to make porous noble metal nanostructures. In a different approach, fusion of preformed noble metal nanoparticles into network structures was also being explored recently. For example, Nadja *et al.* have reported the formation of porous noble metal network structures (aerogel) by treating the preformed citrate-stabilized nanoparticles with hydrogen peroxide[29] for a week or two followed by super critical CO_2 drying to remove the solvent. Grzybowski and co-workers reported the self-assembly of long-chain dithiol-connected, deformable, spherical aggregates into macroscopic nanostructured materials which, on thermal hardening, yields polycrystalline monolith with controlled porosity.[30] All of these processes reported so far are either multistep, nonscalable processes and/or restricted to one or two metals or yield only a very low surface area. Here we are reporting for the first time a remarkably simple, kinetically controlled sodium borohydride reduction process (without any capping agent) to obtain high surface area nanostructured networks of noble metals. Sodium borohydride reduction is an age-old method to obtain metal nanoparticles from their precursors in the presence of a capping agent but seldom used to obtain porous noble metal nanostructures. By carefully controlling the concentration of metal precursors and the sodium borohydride, the fusion of bare metal nuclei formed during the reduction process can be induced to form a three-dimensional sponge-like network of

*Address correspondence to eswar@jncasr.ac.in.

Received for review February 17, 2010 and accepted April 19, 2010.

Published online May 5, 2010.
10.1021/nn100320s

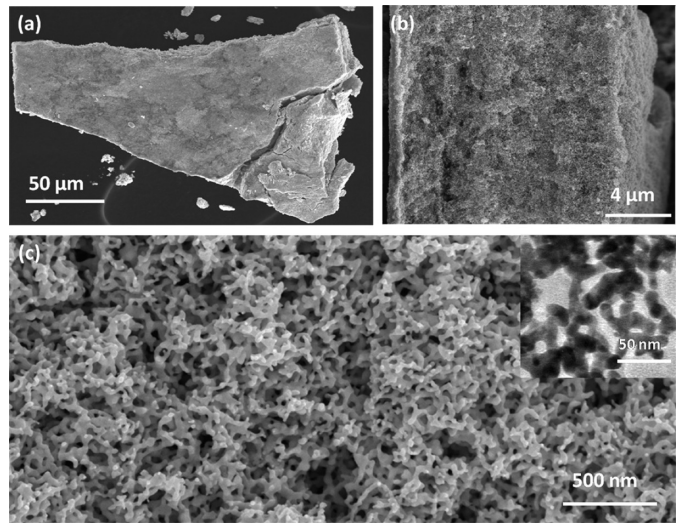

Figure 1. (a) Low-magnification FESEM image of a gold nanosponge in a monolithic form. (b) Cross-sectional view of the gold nanosponge. (c) Higher magnification FESEM image of the gold nanosponge showing porous interconnected networks with ligaments of size 20−50 nm. Inset shows the TEM image of the gold nanosponge.

noble metals instantaneously. The process involves a simple, room temperature reduction of metal salts in water and is, therefore, scalable to any amount. Further, these nanoporous metals for the first time show a true broadband optical limiting behavior[31−33] owing to their network structures which would find applications in optoelectronic nanodevices.

Figure 1a shows the low-magnifigation FESEM image of a gold nanosponge of about 200 μm size obtained by adding 0.1 M auric chloride solution to 0.1 M sodium borohydride solution (1:5 v/v). The cross-sectional image of the nanosponge with 12 μm thickness is shown in Figure 1b. Higher magnification image shows that the nanosponge is made up of porous, interconnected networks (Figure 1c). The sizes of the ligaments creating the nanoporous network are in the range of 20 to 50 nm (Supporting Information 1). Close observation of these networks shows that the ligaments are not of uniform size and often figured with many branches of similar size suggesting their formation through the fusion of nanoparticles. The TEM image (inset of Figure 1c) further confirms that the pores created by the interconnected ligaments are in the order of 50−150 nm. The polycrystalline nature of the sponge observed from the ED pattern also suggests that the nanonetworks were originated from the fusion of nanoparticles (inset of Supporting Information 1). The porous, spongy morphology of gold nanostructure is retained even when the reduction of gold chloride (0.1 M) was carried out with higher concentration of sodium borohydride (2 M) (Figure 2a). Higher magnification FESEM image further shows that the porous networks are made up of nanoligaments of size around 20−50 nm (Figure 2b).

Similar type of spongy network was obtained with silver when silver nitrate (0.1 M) was mixed with sodium borohydride of equimolar concentration in 1:5 volume ratio (Figure 3a). The sizes of ligaments obtained in this case are in the range of 50−80 nm and are well-connected three dimensionally. TEM image (Figure 3b) shows that the sizes of pores are between 50 and 100 nm and are formed by the extended network of fused nanostructure. ED pattern (Figure 3c) further confirms the polycrystalline nature of the silver nanosponge.

Figure 4a shows the spongy structure of Pd made up of thread-like nanoligaments. The network is formed by the fusion of nanoparticles of size around 5 nm (Figure 4b). The interconnected ligaments are significantly smaller in size when compared to Ag and Au ligaments, probably due to the variation in growth kinetics of dif-

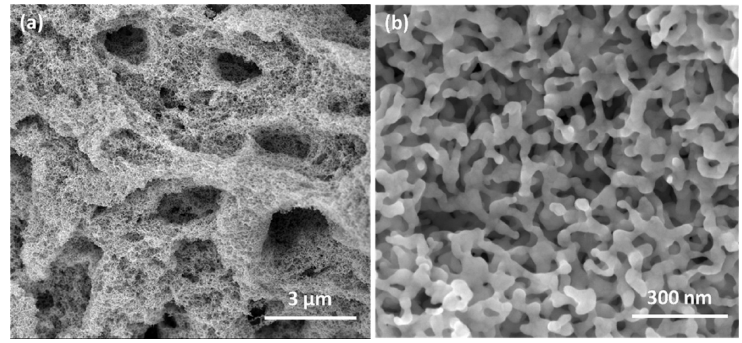

Figure 2. (a) Low-magnification FESEM image of gold nanosponge prepared using 2 M $NaBH_4$ solution showing the spongy networks. (b) Higher magnification FESEM image of the gold nanosponge.

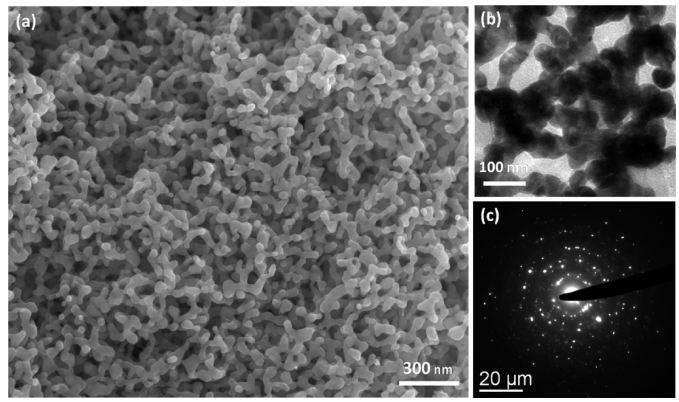

Figure 3. (a) FESEM image of silver nanosponge showing the highly interconnected ligaments. (b) TEM image of the silver nanosponge showing a network of ligaments of size 50−60 nm. (c) ED pattern showing the polycrystallinity of the silver nanosponge.

ferent metal nanoparticles. In a similar way, platinum also forms a three-dimensional network nanostructure shown in Figure 4c. TEM image (Figure 4d) shows that these networks are of the size around 30 nm and are composed of very fine particles of size less than 5 nm. The particles are fused in such a way that even after sonication they stand together and retain the network morphology.

The powder X-ray diffraction pattern (PXRD) shows the peaks corresponding to the cubic phase for all of the metal nanosponges (Figure 5). The peak broadening observed in the XRD patterns is associated with the nanostructured ligaments present in the metal sponges. The nitrogen adsorption−desorption isotherms obtained at liquid nitrogen temperature (77 K) show type II behavior for all of the metal nanosponges. The specific surface area measured using the BET method shows 41, 16, 81, and 51 m^2/g, respectively, for Au, Ag, Pd, and Pt nanosponges (Figure 6). To the best of our knowledge, these are the highest surface areas reported so far for any self-supported Au, Ag, Pd, and Pt nanostructures in one simple, template-free method. Since the networks were formed through the fusion of metal nanoparticles/clusters (of size 5 nm or less in the case of Pd and Pt) emerged during the nucleation step, they were expected to have surface roughness at the nanoscale which would contribute to their high BET surface area.

The UV−vis absorption spectra show near flat absorption for all of the samples for the entire visible region as well as in the IR region associated with the surface plasmon resonance for the extended network nanostructures (Figure 7a). Size- and shape-dependent surface plasmon resonances in Ag and Au nanoparticles were well studied. For example, spherical Ag and Au nanoparticles were known to show one principal plasmon band around 420 and 520 nm, respectively. However, rod-like nanoparticles, depending on the aspect ratio, will show an additional band at higher wavelength associated with the longitudinal plasmon

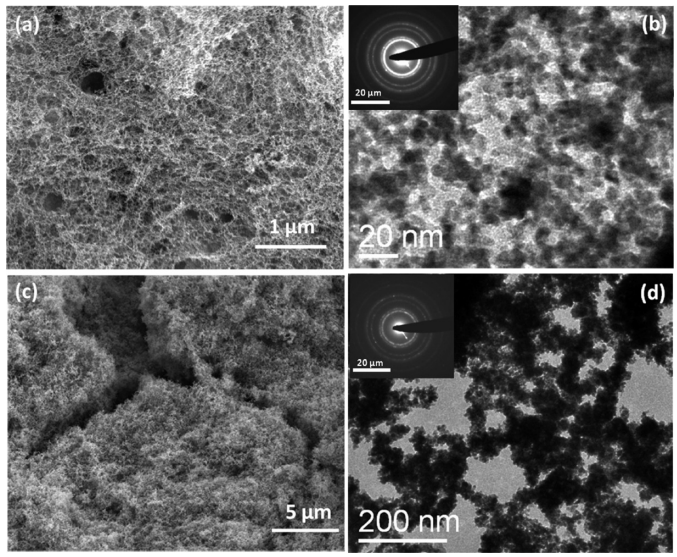

Figure 4. (a) Low-magnification FESEM image of palladium nanosponge. (b) TEM image showing palladium nanoparticles of 5−10 nm size fused to form a network structure. Inset shows its ED pattern. (c) Low-magnification FESEM image showing the platinum nanosponge. (d) TEM image showing the platinum networks made up of nanoparticles of size 5−10 nm. Inset shows its ED pattern.

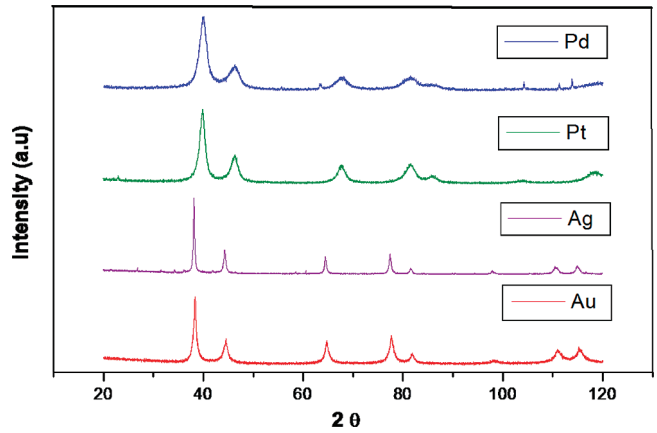

Figure 5. X-ray diffraction pattern of the metal nanosponges.

absorption.[34−36] Since the nanoligaments that constitute the network structures produced in our method have all the length scales, it shows surface plasmon resonance (a convolution of plasmon absorption bands) over the entire visible region as well as in the IR region of the spectrum. This will also explain the near black color observed for the as-prepared materials. Further, these nanosponge powders (Figure 7b) can be pressed into pellet shape without compromising much of its surface area and porosity (Figure 7c). The specific surface areas of porous discs of Au, Ag, Pd, and Pt nanosponges are measured after applying a mechanical pressure of 10 kN (Supporting Information 2), and except for the Ag disk, all of the porous discs retain more or less the same surface area. In the case of Ag, nearly 40% reduction in the surface area was observed at 10 kN pressure. However, the Ag discs made by applying 1 kN pressure show only 25% reduction in surface area (12 m^2/g). Further, the effect of temperature on the nanosponge was studied for silver, which shows a drastic decrease in the surface area with an increase in temperature. This significant reduction in surface area at 500 °C is attributed to the formation of micrometer-sized ligaments due to the sintering of the nanostructure (Supporting Information 3).

The effect of precursor concentration and the reducing agent, $NaBH_4$, on the formation of a porous network was studied using silver nitrate as the model system. Silver nanosponge with high surface area can be readily formed by mixing the solutions of silver nitrate and borohydride of optimum concentration and

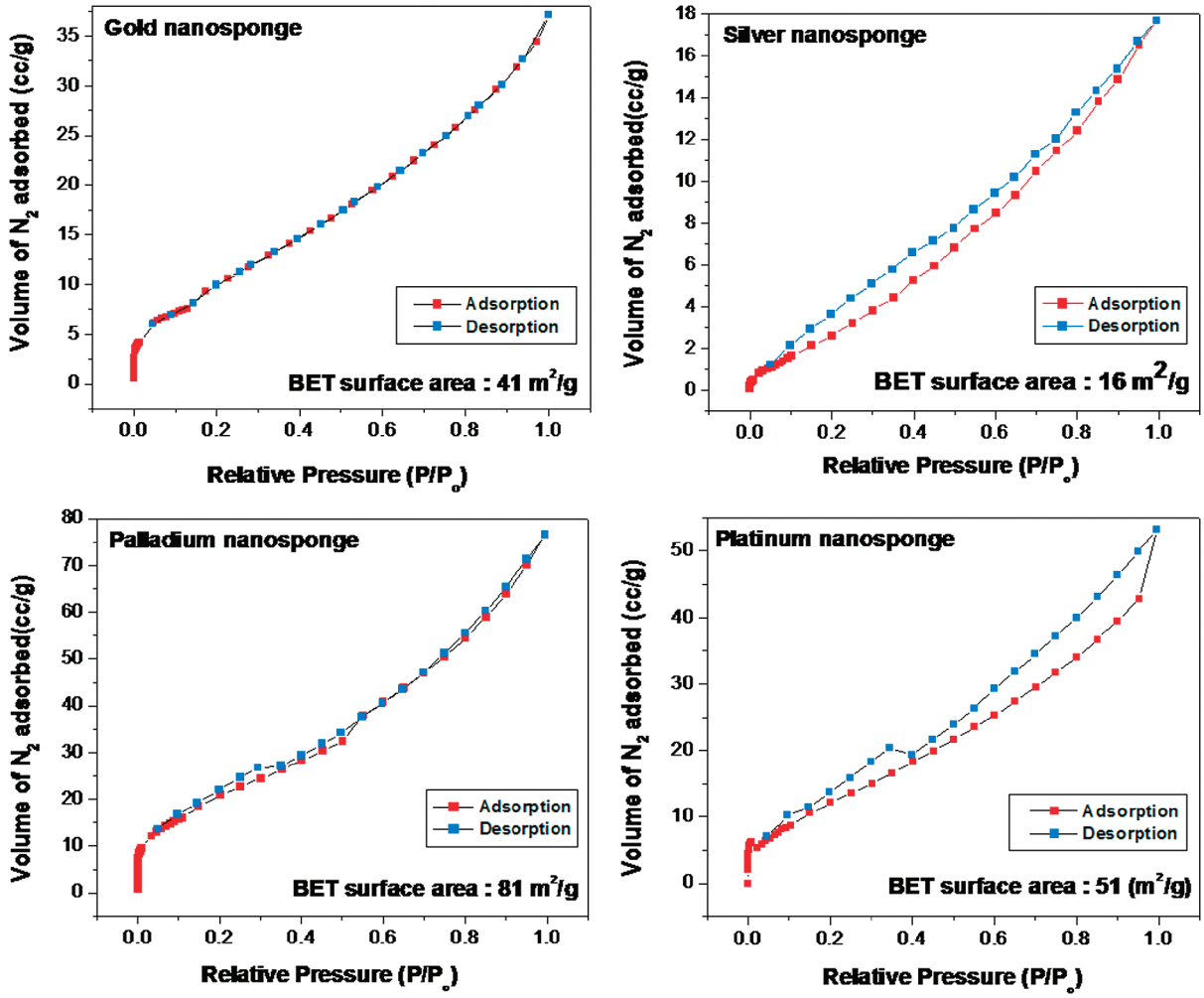

Figure 6. Nitrogen adsorption/desorption isotherms (at 77 K) of the metal nanosponges.

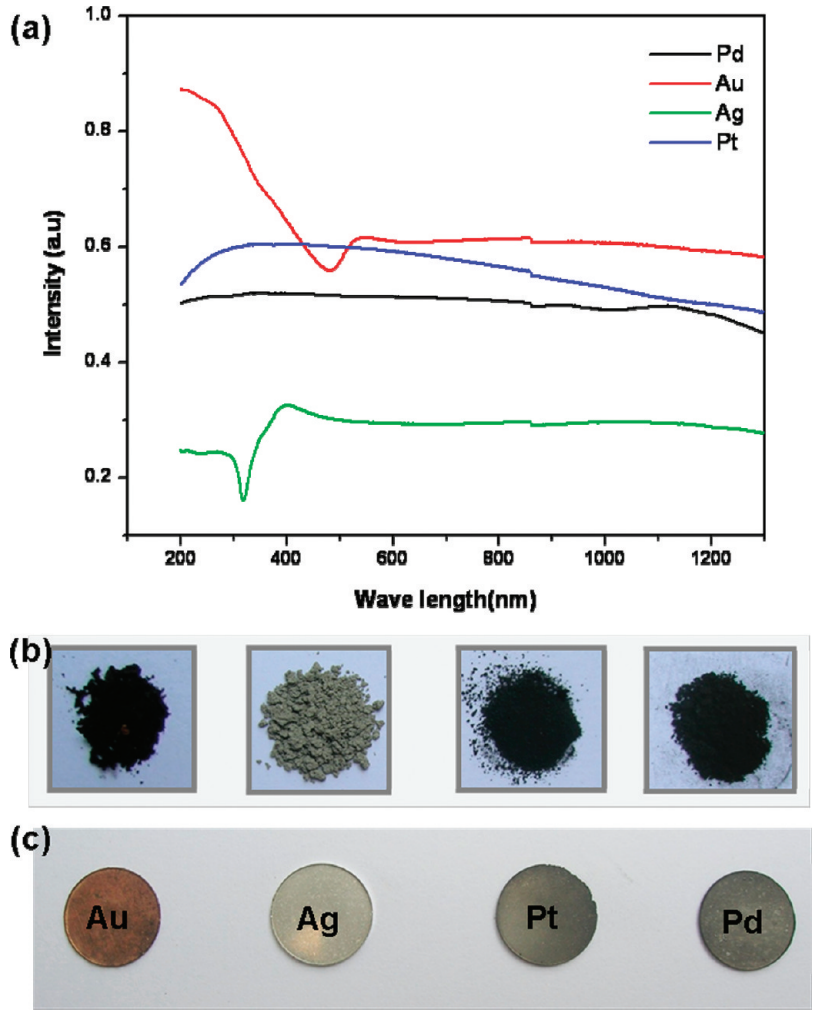

Figure 7. (a) UV−vis spectra of the nanosponges. Photograph of the nanosponges in (b) powder form and (c) pellet forms (applied pressure 10 kN).

amount. If the concentration of silver nitrate is low, around 1.0 mM, the porous silver network does not form, no matter how much sodium borohydride is added (Supporting Information 4). If the concentration of silver nitrate is 0.1 M, addition of an equal volume of 0.1 M sodium borohydride resulted in micrometer-sized ligament silver networks. However, mixing equimolar concentrations (0.1 M and above) of $AgNO_3$ and $NaBH_4$ solutions in a 1:2 v/v ratio gives a very porous network made up of nanosized ligaments. Further, mixing of equal volumes of 0.2 M $AgNO_3$ and 0.1 M $NaBH_4$ solution resulted in micrometer-sized silver particles, and mixing equal volumes of 0.1 M $AgNO_3$ and 0.2 M $NaBH_4$ solution resulted in a spongy nanostructure (Supporting Information 5). It is clear from our studies that the formation of a silver nanosponge depends not only on the initial concentration of silver nitrate and sodium borohydride solution but also on the amount of borohydride ions present in the solution in relation to metal ions. If the concentration of metal ions is below the critical level (*i.e.*, below 0.1 M), it favors the formation of colloidal nanoparticles stabilized in solution. For example, 1.0 mM colorless silver nitrate solution gives yellow to dark green color solution on reduction with sodium borohydride solution of 1 mM or 0.1 M concentration (1:5 v/v ratio).

Addition of sodium borohydride solution to the silver nitrate solution creates many silver nuclei (clusters) which act as the nucleation centers for further growth. The number of nucleation sites (reduced silver sites) formed is directly proportional to the amount of borohydride added. Rapid fusion and growth of the bare nanoparticles leads to interconnected networks of silver (if the concentration of silver nitrate is around 0.1 M and above), which then transforms to a black spongy solid that floats on the solution. It is important to note that these three-dimensional networks are not loosely aggregated nanoparticle structures but are fused architects, as can be seen from the TEM and FESEM images (Figures 2 and 3b) and are stable even after sonication. Drying of the uncapped Ag nanoparticle solution (obtained by mixing 1 mM $AgNO_3$ and 1 mM $NaBH_4$ solution), however, did not give any network structure (Supporting Information 6).

Unlike for metals in the bulk and nanoparticle form, a broad optical absorption is observed for the metal

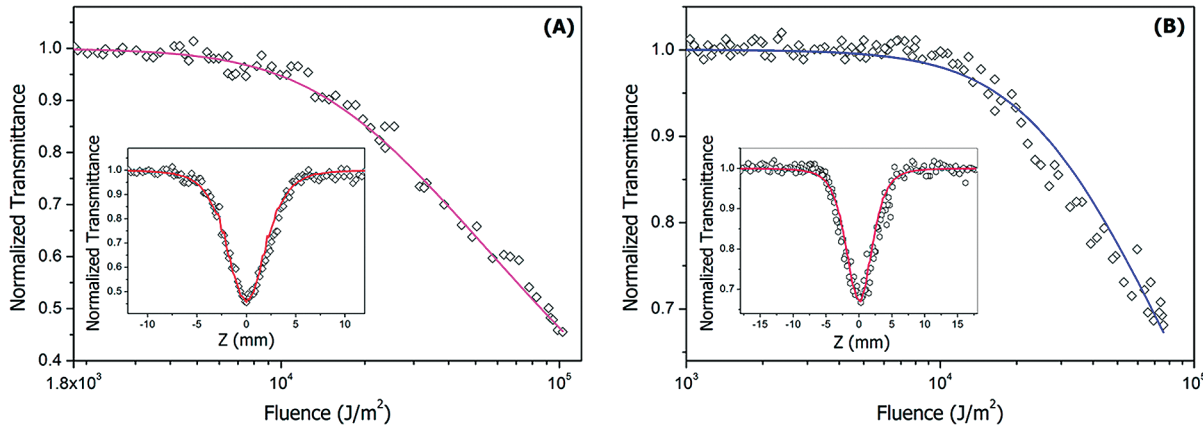

Figure 8. Input laser fluence *vs* normalized transmittance curve for the gold nanosponge sample when excited with (A) 532 nm, 5 ns and (B) 1064 nm, 8 ns laser pulses. Open squares show experimental data, and the solid curve shows the best fit to the data assuming a 3PA process. The insets show the corresponding open-aperture *z*-scan curves.

nanosponges over the entire visible region, which prompted us to study their broadband optical limiting behavior. In a passive optical limiter, the optical transmittance is progressively reduced when the input light intensity increases, which can be used for safeguarding sensitive optical detectors and eyes from accidental exposure to intense laser beams. For instance, an optical limiter based on heavy-metal-substituted naphthalocyanine has been used to protect a silicon CCD array.[37] Some of the optical limiters are referred to as "broadband" devices in literature,[38,39] but to our knowledge, there is no report yet on a nanomaterial-based optical limiter which is truly broadband, that is, capable of limiting laser beams of well-separated wavelengths with similar efficiencies for the same range of input intensities. We observed an optical limiting behavior of nearly the same efficiency in the present nanosponges at 532 and 1064 nm, showing that these are true broadband devices (Supporting Information 7a). This is attributed to the almost flat absorption spectra of the metal nanosponges in the visible and near-IR spectral regions.

The strong optical limiting behavior in gold nanosponge is shown in Figure 8A,B. A three-photon absorption (3PA)-type process gives the best fit to the experimental data (Supporting Information 7b), and the effective three-photon absorption coefficients calculated from the numerical fits are 1.3×10^{-22} m^3/W^2 for 532 nm excitation and 1×10^{-22} m^3/W^2 for 1064 nm. Considering the absorption spectra of the nanosponges and recalling that pure three-photon absorption cross sections are generally very low, it appears that the observed nonlinearity arises from sequential three-photon absorption involving real excited states, rather than from a pure three-photon absorption process. Two-photon absorption followed by excited state absorption is another possibility. Therefore, the nonlinearity can be considered as an "effective" three-photon absorption process. Such absorptive nonlinearities involving real excited states have been reported earlier in C_{60}, carbon nanotube hybrid structures,[40] semiconductors, metal nanoclusters,[33,41] *etc.* To estimate the contribution of nonlinear scattering to the observed optical limiting, we did *z*-scan experiments at relatively lower energies, where nonlinear scattering was negligible (Supporting Information 7c). The gold nanosponge still showed significant optical limiting, confirming that the optical limiting primarily arises from absorptive nonlinearities in the system, though it may be augmented by nonlinear scattering at the higher intensities used.

The nanosponges of gold and silver were also tested for surface-enhanced Raman scattering (SERS) activity and were found to enhance the Raman signals of a known dye, Rhodamine 6G, even at lower concentration (10^{-6} M) (Supporting Information 8a and 8b). Since these nanosponges show broad surface plasmon absorption in the visible and IR regions, the SERS shown by these substrates is not restricted to only one excitation wavelength, as is the case for Au or Ag nanoparticles of particular size. Besides, these porous nanostructures can be easily deposited onto micrometer-sized porous substrates (*e.g.*, ordinary filter papers) and can be used in biofiltration to sieve, identify, and destroy the harmful bacteria and viruses. The antibacterial activity of a silver spongy network deposited on a Whatman filter paper was studied with *Escherichia coli* bacteria (see Experimental Section). The nanosilver-deposited Whatman filter paper shows a significant antibacterial effect, as seen from the inhibition zone it created around the silver nanosponge-embedded filter paper in a bacterial growth medium (Supporting Information 9a and 9b).

In summary, we have synthesized high surface area noble metal nanosponges of Au, Ag, Pd, and Pt by kinetically controlling the simple borohydride reduction process. These 3-D porous nanostructures exhibit efficient broadband optical limiting behavior. Nanosponges of Ag and Au were shown as good substrates for SERS activity. Additionally, the antimicrobial activity of the self-supported nanoporous silver discs or nanoporous silver network incorporated

filter papers could be utilized for water purification, particularly to screen and destroy the harmful pathogens. The synthesis strategy in principle could be extended to obtain nanosponges of other metals (for example, Ru nanostructures prepared by this method were 110 m^2/g), metal oxides, and alloys which could find applications as advanced optical sensors and ultrasensitive detectors.

EXPERIMENTAL SECTION

Gold nanosponge was synthesized by adding 10 mL of an aqueous solution of 0.1 M $HAuCl_4$ (Aldrich) to 50 mL of an aqueous solution of 0.1 M $NaBH_4$ (1:5 v/v ratio of $HAuCl_4/NaBH_4$ solution) with stirring. Addition of auric chloride solution to the borohydride solution resulted in the formation of effervescence (due to the release of hydrogen) with a black spongy solid floating on the reaction medium. The stirring was continued for about 5 min until the entire solution became colorless. The floating solid was filtered and washed with distilled water and dried at room temperature.

In a similar method, Ag, Pd, and Pt nanosponges were synthesized by adding 50 mL of 0.1 M $NaBH_4$ solution with 10 mL of 0.1 M metal precursor solution with stirring. $AgNO_3$, $PdCl_2$, and H_2PtCl_6 were used as the precursors for synthesis of Ag, Pd, and Pt nanosponges, respectively.

***z*-Scan Experiment.** We have carried out the experiments on nonlinear optical properties of the nanosponges using the well-known *z*-scan method (a schematic of the *z*-scan experiment is given in Supporting Information 7d). The *z*-scan is a widely used technique developed by Sheik Bahae *et al.*[42] to measure the nonlinear absorption coefficient and nonlinear refractive index of materials. In the "open-aperture" *z*-scan, a Gaussian laser beam is focused using a convex lens, and its propagation direction is taken as the *z*-axis. The focal point is taken as $z = 0$. This focused beam will have maximum energy density at the focus, which will symmetrically reduce toward either side of it, for the positive and negative values of *z*. The experiment is done by placing the sample in the beam at different positions with respect to the focus (different values of *z*) and measuring the corresponding transmission. The position *versus* transmission curve is known as the open-aperture *z*-scan curve. The sample sees different laser intensity at each position, and hence, the position-dependent transmission data can be converted to the intensity-dependent transmission data. From the *z*-scan curve, the nonlinear absorption coefficient of the sample can be calculated.

In our *z*-scan setup, we used a stepper-motor-controlled linear translation stage to move the sample through the beam in precise steps. The samples were taken in 1 mm glass cuvette (Hellma GMBH). The transmission of the sample at each point was measured by means of two pyroelectric energy probes (RjP7620, Laser Probe Inc.). One energy probe monitored the input energy, while the other monitored the transmitted energy through the sample. The second harmonic output (532 nm) of a Q-switched Nd:YAG laser (Minilite, Continuum) was used for exciting the samples. The nominal pulse width of the laser was 5 ns. For 1064 nm excitation, we used the fundamental output from another Q-switched Nd:YAG laser (Quanta Ray, Spectra Physics). The nominal pulse width at 1064 nm was 8 ns. The pulses were fired in the "single shot" mode, allowing sufficient time between successive pulses to avoid accumulative thermal effects in the sample.

The equation for nonlinear transmission due to a three-photon type absorption is given by[43]

$$T = \frac{(1 - R)^2 \exp(-\alpha L)}{\sqrt{\pi} p_0} \int_{-\infty}^{+\infty} \ln\left[\sqrt{1 + p_0^2 \exp(-2t^2)} + p_0 \exp(-t^2)\right] dt \quad (1)$$

where T is the transmission of the sample, R is the Fresnel reflection coefficient at the sample−air interface, α is the absorption coefficient, and L is the sample length; p_0 is given by $[2\gamma(1 - R)^2 I_0^2 L_{eff}]^{1/2}$, where γ is the three-photon absorption coefficient, and I_0 is the incident intensity. L_{eff} is given by $[1 - \exp(-2\alpha L)]/2\alpha$. By numerically fitting the experimental data to eq 1, the effective three-photon absorption coefficient could be calculated.

Surface-Enhanced Raman Spectroscopy (SERS). The as-prepared nanosponges of silver and gold nanosponges were tested for SERS activity. For this purpose, 20 μL of Rhodamine 6G (both 10^{-4} and 10^{-6} M) was drop casted onto a glass slide containing 10 mg of the nanosponge sample. Raman spectra were recorded at room temperature using a 632 nm HeNe laser as a source. The characteristic signals for Rhodamine 6G were enhanced multifold when observed over the Ag and Au substrates, whereas the Rhodamine 6G dye of 10^{-4} M concentration over the glass slide without the nanosponge could not be detected (Supporting Information 8).

Antibacterial Studies. To study the antibacterial activity of the silver, a silver nanosponge−Whatman composite membrane was prepared by dipping a Whatman filter paper (125 mm ashless circles obtained from Whatman Schleicher & Schuell) in 10 mL of 0.1 M $AgNO_3$ solution for 30 min and followed by dipping it in a 50 mL 0.1 M $NaBH_4$ solution. Immediate reaction resulted in a dark gray colored membrane. The membrane was washed several times with Millipore water and dried at room temperature prior to the study of antibacterial activity.

Antibacterial study was done using *E. coli* (DH5α). The bacteria were inoculated in LB (Luria−Bertani) broth and grown overnight at 37 °C in a shaker incubator. The bacterial cells were plated on an agar medium (1.5% agar plates were made for this purpose). The composite membranes were placed on these plates and incubated overnight at 37 °C. The bacterial growth was observed over the entire plates, except for the zone where the composite membranes were placed. An inhibition zone was clearly seen surrounding the region of the membranes (Supporting Information 9).

Sample Characterization. The morphologies of the samples obtained in all of the experiments were examined with a field-emission scanning electron microscope (FESEM, FEI Nova-Nano SEM-600, The Netherlands) and TEM (JEOL JEM-3010 with an accelerating voltage at 300 kV). Powder X-ray diffraction (XRD) patterns were measured using a RICH-SIEFERT 3000-TT diffractometer employing Cu Kα radiation. N_2 adsorption−desorption isotherms were measured (using nearly 1 g of sample) with a QUANTACHROME AUTOSORB-1C surface-area analyzer at liquid nitrogen temperature (77 K). Absorption studies were carried out using Perkin-Elmer instruments Lambda 900 UV/vis/NIR spectrometer. Raman spectra were recorded with LabRAM HR Raman spectrometer at an excitation wavelength of 632 nm (HeNe laser as source).

Acknowledgment. The authors thank Prof. C. N. R. Rao, FRS for his kind support and encouragement, Prof. G. U. Kulkarni and Prof. Chandrabhas Narayana for useful discussions on XRD and SERS, respectively. The authors acknowledge A. Gomathi for the Raman measurements, Surbhi Dhar for the antibacterial studies, and N. R. Selvi for the FESEM analysis.

Supporting Information Available: Experimental details including adsorption isotherms, SERS studies, and antibacterial studies. This material is available free of charge *via* the Internet at http://pubs.acs.org.

REFERENCES AND NOTES

1. Rolison, D. R. Catalytic Nanoarchitectures—The Importance of Nothing and the Unimportance of Periodicity. *Science* **2003**, *299*, 1698–1701.
2. Steele, B. C. H.; Heinzel, A. Materials for Fuel-Cell Technologies. *Nature* **2001**, *414*, 345–352.

3. Ding, Y.; Chen, M.; Erlebacher, J. Metallic Mesoporous Nanocomposites for Electrocatalysis. *J. Am. Chem. Soc.* **2004**, *126*, 6876–6877.
4. Padilla, A. P.; Rodríguez, J. A.; Saitúa, H. A. Synthesis and Water Ultrafiltration Properties of Silver Membrane Supported on Porous Ceramics. *Desalination* **1997**, *114*, 203–208.
5. Bonroy, K.; Friedt, J. M.; Frederix, F.; Laureyn, W.; Langerock, S.; Campitelli, A.; Sára, M.; Borghs, G.; Goddeeris, B.; Declerck, P. Realization and Characterization of Porous Gold for Increased Protein Coverage on Acoustic Sensors. *Anal. Chem.* **2004**, *76*, 4299–4306.
6. Song, Y. Y.; Zhang, D.; Gao, W.; Xia, X. H. Nonenzymatic Glucose Detection by Using a Three-Dimensionally Ordered, Macroporous Platinum Template. *Chem.—Eur. J.* **2005**, *11*, 2177–2182.
7. Hieda, M.; Garcia, R.; Dixon, M.; Daniel, T.; Allara, D.; Chan, M. H. W. Ultrasensitive Quartz Crystal Microbalance with Porous Gold Electrodes. *Appl. Phys. Lett.* **2004**, *84*, 628–630.
8. Biener, J.; Wittstock, A.; Zepeda-Ruiz, L. A.; Biener, M. M.; Zielasek, V.; Kramer, D.; Viswanath, R. N.; Weissmüller, J.; Bäumer, M.; Hamza, A. V. Surface-Chemistry-Driven Actuation in Nanoporous Gold. *Nat. Mater.* **2009**, *8*, 47–51.
9. Weissmüller, J.; Viswanath, R. N.; Kramer, D.; Zimmer, P.; Würschum, R.; Gleiter, H. Charge-Induced Reversible Strain in a Metal. *Science* **2003**, *300*, 312–315.
10. Yang, P.; Zhao, D.; Margolese, D. I.; Chmelka, B. F.; Stucky, G. D. Generalized Syntheses of Large-Pore Mesoporous Metal Oxides with Semicrystalline Frameworks. *Nature* **1998**, *396*, 152–154.
11. Davis, M. E. Ordered Porous Materials for Emerging Applications. *Nature* **2002**, *417*, 813–821.
12. Zhao, D.; Feng, J.; Huo, Q.; Melosh, N.; Fredrickson, G. H.; Chmelka, B. F.; Stucky, G. D. Triblock Copolymer Syntheses of Mesoporous Silica with Periodic 50 to 300 Angstrom Pores. *Science* **1998**, *279*, 548–552.
13. Bell, A. T. The Impact of Nanoscience on Heterogeneous Catalysis. *Science* **2003**, *299*, 1688–1691.
14. Roucoux, A.; Schulz, J.; Patin, H. Reduced Transition Metal Colloids: A Novel Family of Reusable Catalysts. *Chem. Rev.* **2002**, *102*, 3757–3778.
15. Zielasek, V.; Jürgens, B.; Schulz, C.; Biener, J.; Biener, M. M.; Hamza, A. V.; Bäumer, M. Gold Catalysts: Nanoporous Gold Foams. *Angew. Chem., Int. Ed.* **2006**, *45*, 8241–8244.
16. Xu, C.; Su, J.; Xu, X.; Liu, P.; Zhao, H.; Tian, F.; Ding, Y. Low Temperature CO Oxidation over Unsupported Nanoporous Gold. *J. Am. Chem. Soc.* **2007**, *129*, 42–43.
17. Hughes, M. D.; *et al.* Tunable Gold Catalysis for Selective Hydrocarbon Oxidation under Mild Conditions. *Nature* **2005**, *437*, 1132–1135.
18. Walsh, D.; Arcelli, L.; Ikoma, T.; Tanaka, J.; Mann, S. Dextran Templating for the Synthesis of Metallic and Metal Oxide Sponges. *Nat. Mater.* **2003**, *2*, 386–390.
19. Khan, F.; Eswaramoorthy, M.; Rao, C. N. R. Macroporous Silver Monoliths Using a Simple Surfactant. *Solid State Sci.* **2007**, *9*, 27–31.
20. He, J.; Kunitake, T.; Watanabe, T. Porous and Nonporous Ag Nanostructures Fabricated Using Cellulose Fiber as a Template. *Chem. Commun.* **2005**, 795–796.
21. Attard, G. S.; Gőltner, C. G.; Corker, J. M.; Henke, S.; Templar, R. H. Liquid-Crystal Templates for Nanostructured Metals. *Angew. Chem., Int. Ed. Engl.* **1997**, *36*, 1315–1317.
22. Velev, O. D.; Tessier, P. M.; Lenhoff, A. M.; Kaler, E. W. A Class of Porous Metallic Nanostructures. *Nature* **1999**, *401*, 548.
23. Erlebacher, J.; Aziz, M. J.; Karma, A.; Dimitrov, N.; Sieradzki, K. Evolution of Nanoporosity in Dealloying. *Nature* **2001**, *410*, 450–453.
24. Ding, Y.; Erlebacher, J. Nanoporous Metals with Controlled Multimodal Pore Size Distribution. *J. Am. Chem. Soc.* **2003**, *125*, 7772–7773.
25. Qin, G. W.; Liu, J.; Balaji, T.; Xu, X.; Matsunaga, H.; Hakuta, Y.; Zuo, L.; Raveendran, P. A Facile and Template-Free Method to Prepare Mesoporous Gold Sponge and Its Pore Size Control. *J. Phys. Chem. C* **2008**, *112*, 10352–10358.
26. Ramanath, G.; D'Arcy-Gall, J.; Maddanimath, T.; Ellis, A. V.; Ganesan, P. G.; Goswami, R.; Kumar, A.; Vijayamohanan, K. Templateless Room-Temperature Assembly of Nanowire Networks from Nanoparticles. *Langmuir* **2004**, *20*, 5583–5587.
27. Vishwanath, B.; Patra, S.; Munichandraiah, N.; Ravishankar, N. Nanoporous Pt with High Surface Area by Reaction-Limited Aggregation of Nanoparticles. *Langmuir* **2009**, *25*, 3115–3121.
28. Song, Y.; Garcia, R. M.; Dorin, R. M.; Wang, H.; Qiu, Y.; Coker, E. N.; Steen, W. A.; Miller, J. E.; Shelnutt, J. A. Synthesis of Platinum Nanowire Networks Using a Soft Template. *Nano Lett.* **2007**, *7*, 3650–3655.
29. Bigall, N. C.; Herrmann, A-K; Vogel, M.; Rose, M.; Simon, P.; Carrillo-Cabrera, W.; Dorfs, D.; Kaskel, S.; Gaponik, N.; Eychmüller, A. Hydrogels and Aerogels from Noble Metal Nanoparticles. *Angew. Chem., Int. Ed.* **2009**, *48*, 9731–9734.
30. Klajn, R.; Bishop, K. J. M.; Fialkowski, M.; Paszewski, M.; Campbell, C. J.; Gray, T. P.; Grzybowski, B. A. Plastic and Moldable Metals by Self-Assembly of Sticky Nanoparticle Aggregates. *Science* **2007**, *316*, 261–264.
31. Tutt, L. W.; Kost, A. Optical Limiting Performance of C_{60} And C_{70} Solutions. *Nature* **1992**, *356*, 225–226.
32. Perry, J. W.; Mansour, K.; Lee, I.-Y. S.; Wu, X.-L.; Bedworth, P. V.; Chen, C.-T.; Ng, D.; Marder, S. R.; Miles, P.; Wada, T.; Sasabe, H. Organic Optical Limiter with a Strong Nonlinear Absorptive Response. *Science* **1996**, *273*, 1533–1536.
33. Tutt, L. W.; Boggess, T. F. A Review of Optical Limiting Mechanisms and Devices Using Organics, Fullerenes, Semiconductors, and Other Materials. *Prog. Quantum Electron.* **1993**, *17*, 299–338.
34. Tao, A.; Kim, F.; Hess, C.; Goldberger, J.; He, R.; Sun, Y.; Xia, Y.; Yang, P. Langmuir−Blodgett Silver Nanowire Monolayers for Molecular Sensing Using Surface-Enhanced Raman Spectroscopy. *Nano Lett.* **2003**, *3*, 1229–1233.
35. Orendoriff, C. J.; Gearheart, L.; Jana, N. R.; Murphy, C. J. Aspect Ratio Dependence on Surface Enhanced Raman Scattering Using Silver and Gold Nanorod Substrates. *Phys. Chem. Chem. Phys.* **2006**, *8*, 165–170.
36. Eutis, S.; El-Sayed, M. A. Why Gold Nanoparticles Are More Precious than Pretty Gold:Noble Metal Surface Plasmon Resonance and Its Enhancement of the Radiative and Nonradiative Properties of Nanocrystals of Different Shapes. *Chem. Soc. Rev.* **2006**, *35*, 209–217.
37. Dentan, V.; Feneyrou, P.; Soyer, F.; Vergnolle, M.; Le Barny, P.; Robin, Ph. Broadband Optical Limiting and CCD Sensor Protection from Nanosecond-Pulsed Laser Threat with Reverse Saturable Absorbers. *Mater. Res. Soc. Symp. Proc.* **1997**, *479*, 261–267.
38. Wang, J.; Hernandez, Y.; Lotya, M.; Coleman, J. N.; Blau, W. J. Broadband Nonlinear Optical Response of Graphene Dispersions. *Adv. Mater.* **2009**, *21*, 2430.
39. Sun, X.; Yu, R. Q.; Xu, G. Q.; Hor, T. S. A.; Ji, W. Broadband Optical Limiting with Multiwalled Carbon Nanotubes. *Appl. Phys. Lett.* **1998**, *73*, 3632–3634.
40. Narayanan, T. N.; Sandeep, C. S. S.; Shaijumon, M. M.; Ajayan, P. M.; Philip, R.; Anantharaman, M. R. The Synthesis of High Coercivity Cobalt-in-Carbon Nanotube Hybrid Structures and Their Optical Limiting Properties. *Nanotechnology* **2009**, *20*, 285702.
41. Philip, R.; Ravindrakumar, G.; Sandhyarani, N.; Pradeep, T. Picosecond Optical Nonlinearity in Monolayer-Protected Gold, Silver, and Gold−Silver Alloy Nanoclusters. *Phys. Rev. B* **2000**, *62*, 13160–13166.
42. Sheik Bahae, M.; Said, A. A.; Wei, T. M.; Hagan, D. J.; Vanstryland, E. W. Sensitive Measuremens of Optical Nonlinearities Using a Single Beam. *IEEE J. Quantum Electron.* **1990**, *26*, 760–769.
43. Sutherland, R. L. *Hand Book of Nonlinear Optics*, 2nd ed.; Marcel Dekker: New York, 2003; p 591.